Glowacki, D. R., Rose, R. A., Greaves, S. J., Orr-Ewing, A. J., & Harvey, J. N. (2011). Ultrafast energy flow in the wake of solution phase bimolecular reactions. Nature Chemistry, 3(11), 850 - 855. 10.1038/nchem.1154

Ultrafast energy flow in the wake of solution phase bimolecular reactions

David R. Glowacki,* Rebecca A. Rose, Stuart J. Greaves, Andrew J. Orr-Ewing, and Jeremy N. Harvey*

School of Chemistry, University of Bristol, Bristol BS8 1TS, United Kingdom

david.r.glowacki@bristol.ac.uk, Jeremy.Harvey@bristol.ac.uk

Abstract

In this study, we elucidate the microscopic details of how ultrafast rearrangements in liquid structure affect energy flow in the wake of a thermal bimolecular reaction. Using non-equilibrium molecular dynamics to analyze ultrafast experimental data, we examined the reaction of CN + c-C_6H_{12} → HCN + c-C_6H_{11} in CH_2Cl_2 solvent, which produces vibrationally hot HCN. Both theory and experiment show that HCN relaxation follows multiple timescales, which arises because of time-dependent energy transfer efficiencies as HCN experiences an effective structural change in its solvent environment, and results in an apparent breakdown of linear response theory. At short times, HCN is locked within a solvated supermolecular complex with its co-product, and relaxation is fast. At longer times, HCN diffuses away from its co-product, and relaxation is slower. These results allow us to begin forming a detailed picture of the interplay between ultrafast fluctuations in solvent structure and thermal solution phase chemistry.

Nearly all chemical reactions involve some degree of vibrational energy transfer.[1] Because typical bond strengths are on the order of tens of kcal mol^{-1}, surmounting the energy barriers associated with bond-breaking and forming at ambient temperatures requires the localization of significant amounts of energy in a particular vibrational mode. Set against this requirement is the fact that equilibrium statistical mechanics tells us that energy is statistically randomized in all of the states of the system at long times. Thus, understanding the origins and timescales of non-equilibrium energy localization for condensed phase systems with high state densities remains a critical issue in our attempts to develop predictive models of condensed phase chemical reactivity. The predominant model guiding our understanding of condensed phase non-equilibrium dynamics is linear response theory (LRT),[2] which arises from the fluctuation-dissipation theorem, and amounts to a statement that the relaxation of a system following spontaneous fluctuations from equilibrium is indistinguishable from relaxation that follows from external preparation of a non-equilibrium system.[3] Despite a few exceptions,[4,5,6,7,8,9,10] LRT provides a robust framework for understanding relaxation to equilibrium within liquids.

In this article, we investigate the vibrational relaxation of HCN formed through a bimolecular H abstraction reaction in CH_2Cl_2 solvent, the products of which are illustrated in Figure 1:

$$CN + c\text{-}C_6H_{12} \rightarrow HCN + c\text{-}C_6H_{11} \qquad (R1)$$

The energies involved in (R1) are characteristic of typical thermal reaction energies, and well within a regime where one might expect relaxation of the vibrationally excited nascent HCN to follow LRT. However, as we will show, the HCN experiences ultrafast changes in the structure of its environment following (R1). This results in multiple LRT HCN relaxation regimes, which must be properly accounted for in order to adequately describe our theoretical and experimental observations over the range of post-reaction timescales. While examples of non-linear responses have been highlighted for solvation dynamics,[4,7,9] electron transfer,[6,8] and photochemistry,[5,10] this study employing computational simulations of recent experimental data is the first time (to our knowledge) that such results have been shown for the case of a thermal chemical reaction involving an atomic rearrangement.

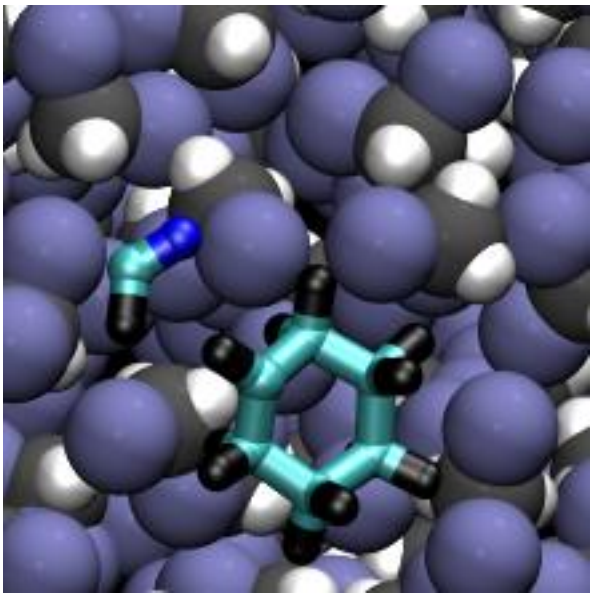

Figure 1. MD snapshot of (R1) products within a CH_2Cl_2 solvent cavity

Linear Response Interpretation of the Experiments

It has been known for some time that gas phase abstraction reactions of CN with alkanes like (R1) yield HCN which is vibrationally excited in both its CH stretching (00*n*) and HCN bending (0*n*0) modes.[11,12,13,14] In recently published experimental and theoretical work,[15,16] CN radicals were generated through ICN photolysis, and the time profile of the vibrational state populations of the nascent HCN generated in (R1) was monitored using ultrafast infrared lasers. The results showed significant HCN vibrational excitation. Gas and solution phase MD simulations suggest that the product energy deposition into HCN for (R1) in a CH_2Cl_2 solvent at short times is nearly identical – i.e., the product energy specificity is preserved in the corresponding solution phase reaction following passage over the abstraction TS.[16] At longer times, however, the gas phase and solution phase results differ: whereas the energy of the HCN and *c*-C_6H_{11} co-products is conserved in the gas phase, it relaxes to thermal equilibrium in solution.

In our previous work, the experimental time traces obtained from (R1) were fit using the kinetic model in Figure 2a, in which the HCN(0*n*1) and HCN(001) relaxation rates were constrained to the experimentally measured k_6 and k_7 decay rates observed from ultrafast pump-probe experiments of vibrationally excited HCN relaxing in CH_2Cl_2 solvent with 1 M *c*-C_6H_{12}. This model implicitly assumes that HCN vibrational relaxation follows standard time-independent LRT – i.e., *the rate of relaxation of HCN to equilibrium is independent of the means through which it was initially prepared, whether via laser pulse or by* (*R1*). While the kinetic model in Figure 2a gives good fits to the experimentally

observed changes in optical density (OD) at long times, Figure 2b shows that the fits are less satisfactory at short times, where the negative ODs indicate HCN(000) and HCN(0*n*0) population inversions whose magnitudes are underestimated.

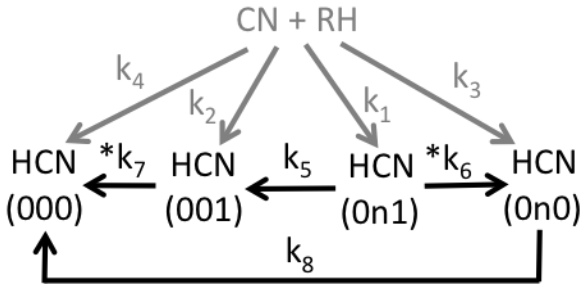

Figure 2a. Simple kinetic model (which implicitly assumes LRT behaviour) used to rationalize the experimentally measured time profiles in Figure 2b. * denotes that the fit parameters were not floated, but fixed to experimental IR pump-probe measurements

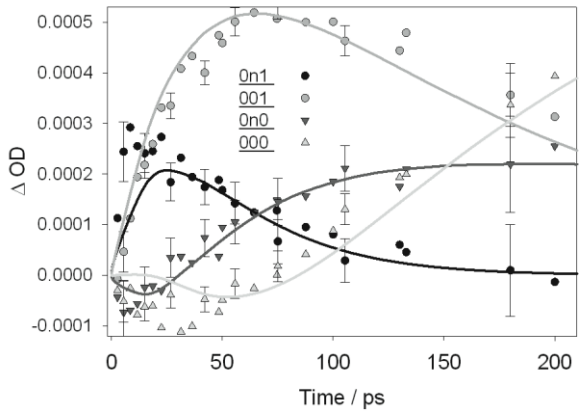

Figure 2b. Representative experimental trace showing the changes in optical density (OD) for HCN(0*n*0), (001), (0*n*1), and (000). The solid lines show the fit obtained using the kinetic model shown in Figure 2a

One possible explanation for why the model in Figure 2a underestimates the degree of population inversion at short times is that HCN (002) is formed along with the nascent HCN(001). However, fitting the data using a numerical integration scheme which includes this channel requires that relaxation from HCN(002) into HCN(001) is at least an order of magnitude faster than the (001) relaxation, and that more than 50% of the HCN produced in (R1) is in the (002) state. These conclusions are at odds with (i) results obtained from our MD simulations (see SI), which show that the energy relaxation timescales of (001)←(002) and (000)←(001) are the same within statistical error, and (ii) our experiments, which suggest an upper limit of 10% for the HCN (002) yield.[15]

NEMD Simulations: Mapping Energy Flow

Further insight into the experimental results and the origin of the short-time disagreement shown in Figure 2b was obtained by carrying out a number of molecular dynamics simulations in a periodic box of 125 fully flexible CH_2Cl_2 solvent molecules, which allowed us to examine the time-dependent energy in the HCN normal modes and the cyclohexyl co-product in more detail than was experimentally possible. Initially, we performed the following two sets of classical dynamics simulations: (1) 250 non-reactive NVE trajectories in which we investigated the relaxation of vibrationally excited HCN(001) in neat CH_2Cl_2 solvent, and (2) 250 reactive trajectories using a recently developed analytic reactive force field for CN + *c*-C_6H_{12} → HCN + *c*-C_6H_{11} in CH_2Cl_2.[16] For each trajectory, time-dependent C-H stretch normal mode energies, $E_{CH}(t)$, were obtained by projecting the molecular Cartesian coordinates and momenta into the normal mode frame of molecular equilibrium geometries. The results were then averaged over all 250 trajectories to obtain ensemble averaged energies, $\overline{E_{CH}}(t)$, which are shown in Figure 3.

Figure 3 indicates that the $\overline{E_{CH}}(t)$ decay in neat CH_2Cl_2 may be fit using a single exponential with a time constant of 736 ± 531 ps^{-1}. In marked contrast, the $\overline{E_{CH}}(t)$ profile obtained when HCN is formed via (R1) shows multiple decay timescales – with a fast initial decay and a slower long time decay. Fitting these data with a biexponential gives a fast decay time constant, τ_1, of 7.0 ± 0.2 ps, and a slow time constant, τ_2, of 204 ± 33 ps. The latter is close to the value of 144 ± 8 ps obtained from experimental IR pump-probe measurements of HCN (001) decay in a CH_2Cl_2 solvent and 1 M *c*-C_6H_{12}.[15]

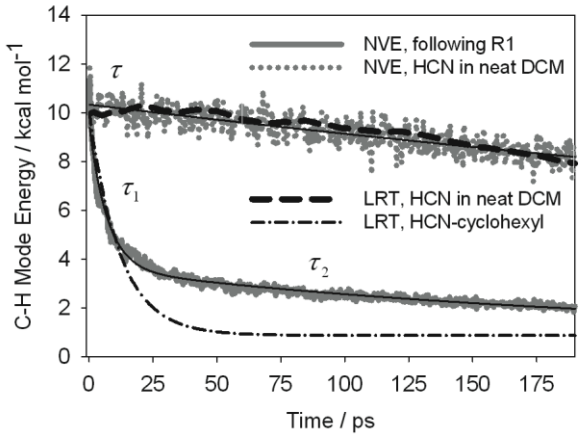

Figure 3. Time-dependence of the HCN C–H stretching energy obtained from averaging over 250 NEMD simulations carried out in: (i) neat CH_2Cl_2 solvent (solid black line fit to a single exponential decay curve with time constant τ); (ii) following abstraction of an H atom from *c*-C_6H_{12} in CH_2Cl_2 solvent (solid black line fit to a biexponential decay curve with time constants τ_1 and τ_2). Also shown are the LRT predictions obtained from a single equilibrium trajectory of HCN relaxation (a) in neat CH_2Cl_2, and (b) complexed to c-C_6H_{11} in CH_2Cl_2

The results of the simulations discussed above were compared to the predictions of time-independent LRT in both the presence and absence of c-C_6H_{11}. For this purpose, we performed two different classical dynamics simulations: (a) a single 2 ns NVE simulation of HCN in CH_2Cl_2, and (b) a single 2 ns NVE simulation in CH_2Cl_2 with HCN and c-C_6H_{11} radical constrained using the AXD algorithm[17,18] to have a center of mass separation less than 5.7 Å. In each case, the initial coordinates and momenta were obtained by sampling a 298K ensemble, and subsequent correlation functions of E_{CH}, $C(t)$, were calculated as:

$$C(t) = \langle E_{CH}(t_0) E_{CH}(t_0 + t) \rangle - \langle E_{CH} \rangle^2 \qquad \text{Eq (1a)}$$

where the angle brackets denote averaging over the whole trajectory, so that e.g., $\langle E_{CH} \rangle$, is the average time-independent C–H stretching energy at thermal equilibrium, and t_0 represents all possible start times within the trajectory. The LRT prediction was calculated using $C(t)$ as

$$\frac{\overline{E_{CH}}(t)-\langle E_{CH}\rangle}{\overline{E_{CH}}(0)-\langle E_{CH}\rangle}=\frac{C(t)}{C(0)} \qquad \text{Eq (1b)}$$

As shown in Fig 3, the time-dependent energy profiles of excited HCN in neat CH_2Cl_2 averaged over 250 trajectories decay in close agreement with single trajectory predictions based on LRT calculated from Eq (1b), showing that an excitation of 10 kcal mol^{-1} is not so large a perturbation as to make the CH response non-linear.

Figure 3 shows that neither of the LRT correlation functions – in either the presence or absence of c-C_6H_{11}, fully explains the observed decay trace following (R1). At short times, it appears that LRT for the HCN-cyclohexyl complex correctly captures the physics, while at longer times, the decay approaches the LRT predictions for HCN decay in neat CH_2Cl_2. The question that arises is as follows: Why is there such an apparently strong violation of simple LRT for relaxation of the CH mode when HCN is formed in (R1) – and specifically, why is the energy relaxation at short times following reaction so much faster than at longer times? The answer lies in recognizing that we must not only consider energy deposition in the nascent HCN formed in (R1), but also in its *c*-C_6H_{11} co-product. Accordingly, we used the normal mode projection algorithm described above to examine $\overline{E_{C_6H_{11}}}(t)$, the time dependent vibrational energy content of *c*-C_6H_{11} following its formation in (R1). The results averaged over 250 reactive trajectories in both the gas phase and in CH_2Cl_2 solvent are shown in Figure 4.

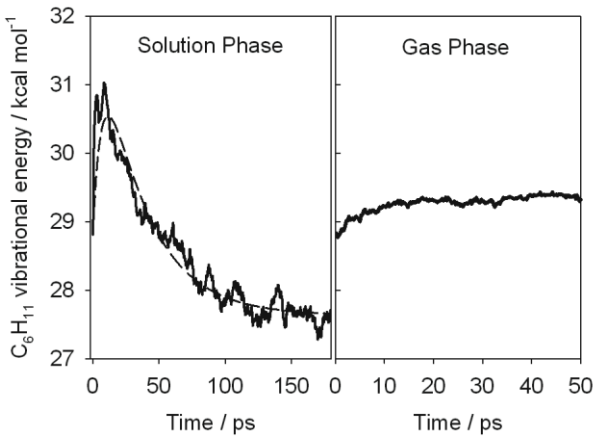

Figure 4. Comparison of the total vibrational energy of the nascent *c*-C_6H_{11} in both the gas phase and solution phase reactive dynamics simulations. The solution phase panel shows the fit (dashed line) obtained using the simple energy flow kinetic model described in the text

Whereas $\overline{E_{C_6H_{11}}}(t)$ is more or less constant with time in gas phase simulations (right hand panel), it shows a significantly different energy profile in the solution phase dynamics (left hand panel), with a rise at short times followed by a subsequent decay. The profile of $\overline{E_{C_6H_{11}}}(t)$ following (R1) may be reasonably well described by the following simple irreversible kinetic scheme, which maps the flow of excess vibrational energy between HCN, *c*-C_6H_{11}, and the CH_2Cl_2 solvent bath:

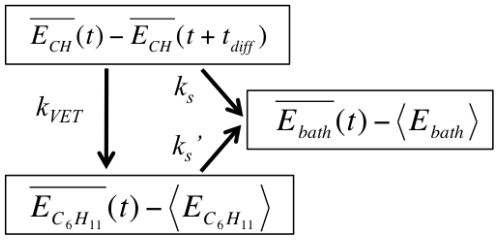

where k_{VET} is the rate coefficient for flow of excess CH stretching vibrational energy, $\overline{E_{CH}}$, from HCN to *c*-C_6H_{11}, k_s is the rate coefficient for flow of CH stretch energy in HCN to the CH_2Cl_2 solvent bath in the presence of *c*-C_6H_{11}, k_s' is the rate coefficient for energy flow from vibrationally excited *c*-C_6H_{11} to the solvent bath in the presence of HCN, and t_{diff} is the time at which the HCN has diffused far enough away from *c*-C_6H_{11} that the k_{VET} and k_s pathways effectively shut off. Energy transfer from HCN to solvent in the absence of c-C_6H_{11}, as shown in Fig. 3, is slow enough to be neglected at times smaller than t_{diff}. The rate equations that make up the kinetic mechanism for mapping energy flow in the immediate aftermath of (R1) may be solved using an integrating factor to give an analytic solution for the ensemble-averaged time dependent energy in *c*-C_6H_{11}:

$$\begin{aligned}\overline{E_{C_6H_{11}}}(t) &= A\exp[-(k_{VET}+k_s)t]+\\ &\quad B\exp(-k_{VET}t)+E_{C_6H_{11}}(\infty)\\ A &= \frac{k_{VET}\left(\overline{E_{CH}}(0)-\overline{E_{CH}}(t_{diff})\right)}{k_s'-k_{VET}-k_s}\\ B &= \overline{E_{C_6H_{11}}}(0)-\langle E_{C_6H_{11}}\rangle - A\end{aligned} \qquad \text{Eq (2)}$$

The left hand panel of Figure 4 shows fits obtained using Eq 2 with the following constraints: (i) $k_{VET} + k_s$ is equal to $1/\tau_1$ (where τ_1, shown in Figure 3, is the time constant for energy decay from the nascent HCN following abstraction), and (ii) the average initial energy (t = 0) in the *c*-C_6H_{11} fragment is 28.8 kcal mol^{-1}. The parameters producing the fit are in Table 1.

Parameter	Value
k_{VET}	0.076 ps^{-1}
k_s	0.067 ps^{-1}
k_s'	0.030 ps^{-1}
$\overline{E_{CH}}(0)-\overline{E_{CH}}(t_{diff})$	6.0 kcal mol^{-1}
$\langle E_{C_6H_{11}}\rangle$	27.6 kcal mol^{-1}

Table 1. Parameters obtained from fitting the Figure 4 data using Eq (2)

The values of the rate coefficients in Table 1 show that the fast energy transfer from HCN to *c*-C_6H_{11} has a time constant of ~15 ps, during which time the relative separation between the HCN and *c*-C_6H_{11} centers of mass following (R1) increases from an initial value of ~5 Å to ~6.3 Å. Another interesting fitting result is the fact that the rate coefficient for energy transfer from HCN to solvent in the presence of *c*-C_6H_{11}, k_s, is similar in value to k_{VET}. While a reasonable, albeit much less accurate fit can be obtained by setting k_s = 0 (see SI), this suggests that *c*-C_6H_{11} serves two roles with respect to HCN energy relaxation: it is an efficient acceptor of vibrational energy from HCN, and it also mediates efficient energy transfer from HCN to the CH_2Cl_2 solvent.[19,20] The difference between $\overline{E_{CH}}(0)$, which is ~10.5 kcal mol^{-1}, and $\overline{E_{CH}}(t_{diff})$ is ~6 kcal mol^{-1}, in reasonable agreement with extrapolation of the τ_2 decay in Figure 3 to t = 0.

A microscopic picture of post reaction energy transfer thus emerges: immediately following reaction, the vibrational energy distributions in both HCN and *c*-C_6H_{11} are similar to their gas phase values. At short times, energy relaxation of the nascent HCN is efficient given its proximity to *c*-C_6H_{11}, which soaks up vibrational energy from the HCN, and also facilitates energy transfer to the solvent. In this regime, the LRT correlation function obtained from locking HCN and cyclohexyl in close proximity gives a good representation of the dynamics. As the HCN and *c*-C_6H_{11} diffuse away from one another, HCN energy relaxation to the solvent bath becomes less efficient, approaching the relaxation that would be expected on the basis of the LRT correlation functions obtained in neat CH_2Cl_2. In the wake of (R1), the hot nascent HCN moves between the limits of these two LRT regimes.

Experimental Observations

Having established that the HCN decay follows multiple timescales and the corresponding inadequacy of a simple time-stationary LRT treatment, we revisited the experimental data in Figure 2b. A simple improvement of the kinetic model in Figure 2a is shown in Figure 5a. It incorporates the two different LRT regimes which the HCN experiences in the wake of (R1). The first occurs when the nascent HCN undergoes efficient energy relaxation within a caged super-molecular post-reaction complex with *c*-C_6H_{11} (R in Figure 5a). The second occurs when the super-molecular complex has undergone diffusional dissociation into the solvent. Figure 5a model includes two parameters beyond those in Figure 2a: (i) k_d, which is a rate coefficient representing transfer from the HCN-cyclohexyl LRT regime to that in the bulk solvent as a result of diffusion, and (ii) *s*, which accounts for the fact that HCN energy relaxation in the presence of *c*-C_6H_{11} is *s* times faster than in free CH_2Cl_2.

Using the kinetic model in Figure 5a, we refit the experimental data using a numerical integration procedure. The fit is shown in Figure 5b, and the floated average parameters obtained from fits carried out on different data sets are given in Table 2,

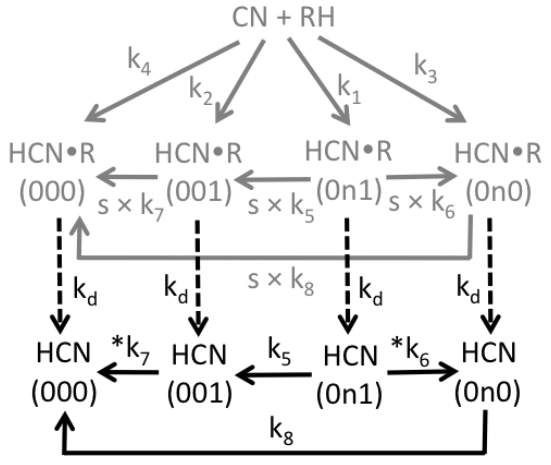

Figure 5a. Kinetic model which accounts for the different LRT regimes that HCN experiences. Grey represents dynamics when the nascent HCN is complexed to R (*c*-C_6H_{11}) within the initial solvent cage, the dashed line represents diffusion of HCN away from R with rate coefficient k_d, and black represents subsequent dynamics of HCN in the bulk solvent. * has the same meaning as in Figure 2a.

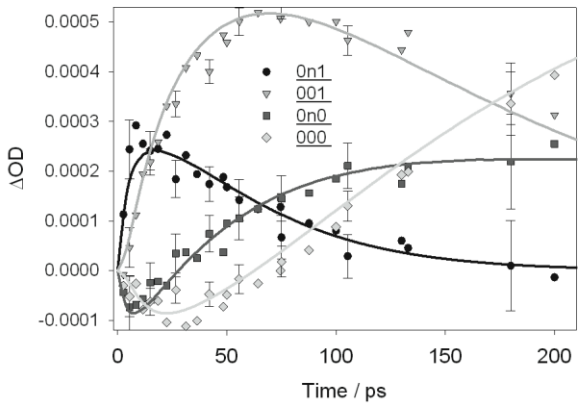

Figure 5b. Same as Figure 1, with the difference that the solid lines now show the fit obtained using the improved kinetic model in Figure 5a

Parameter	Value
k_1	$(2.20 \pm 0.25) \times 10^{-2}$ ps^{-1}
k_2	$(4.56 \pm 0.69) \times 10^{-3}$ ps^{-1}
k_3	$(2.17 \pm 1.10) \times 10^{-3}$ ps^{-1}
k_4	$(9.86 \pm 0.83) \times 10^{-4}$ ps^{-1}
s	10.9 ± 1.7
k_d	$(8.89 \pm 2.86) \times 10^{-2}$ ps^{-1}
k_5	$(7.80 \pm 1.03) \times 10^{-3}$ ps^{-1}
k_8	$(3.64 \pm 0.67) \times 10^{-4}$ ps^{-1}

Table 2. Parameters obtained from average fits over a number of experimental data sets using Figure 5a; errors are 95% confidence limits

At long times, the results of fitting Figure 5a to the time-resolved experimental data differ little from those obtained with Figure 2a. The real improvement, shown in Figure 5b, is that Figure 5a provides a significantly better representation of the short-time HCN (000) and HCN (0*v*0) population inversions – *an improvement which is exactly within the time domain where our previous time-stationary LRT fitting procedure was most inadequate for describing HCN energy relaxation in the presence of c-C_6H_{11}.* The parameters in Table 2 indicate that the respective branching ratios for the pathways corresponding to k_1, k_2, k_3, and k_4 are 0.74, 0.16, 0.07, and 0.03, suggesting (R1) predominantly forms HCN which has both bend and stretch excitation, in good agreement with detailed analyses of the energy deposition in HCN obtained from both gas and solution phase molecular dynamics simulations.[16] The rate coefficient for diffusion of HCN away from *c*-C_6H_{11} in CH_2Cl_2, k_d, is compatible with experimental measurements of the self-diffusion coefficient of CH_2Cl_2 at 298K.[21] Over a time of $1/k_d$, the one-dimensional CH_2Cl_2 self-diffusion distance is on the order of 6 Å. The scaling factor, *s*, has a best fit value of 10.9 ± 1.7. Within error bars, this is within a factor of two of the value of 29.1 ± 4.8 suggested by the MD results in Figure 3. This level of agreement is reasonable, considering the approximations we have made in treating the energy transfer process with classical mechanics and an MMFF force field.

Discussion and Conclusions

The combined theoretical and experimental work presented herein shows that ultrafast experimental observations of energy relaxation of HCN in the wake of a solution phase bimolecular

reaction occurs on multiple timescales. There are two relevant LRT limits – one for a solvent caged HCN-cyclohexyl complex, and one for HCN in bulk CH_2Cl_2. As HCN diffuses out of the solvent caged supermolecular co-product complex into the bulk, the structure of its effective solvent environment changes, and the initial energy transfer efficiency diminishes. For the reverse reaction, which has a much higher barrier, microscopic reversibility dictates that similar effects will occur in the supermolecular reactant complex.

This work provides an exciting link between results obtained from MD simulations, and what appear to be implicit experimental observations of ultrafast solvent structural dynamics. It sheds light on the microscopic origins and time dependence of energy transfer in chemical reactions, and suggests that: (i) kinetic models derived from a simple time-independent LRT approach are not necessarily transferable to systems that feature atomic reaction dynamics, and more sophisticated treatments are required;[9,22] (ii) models which represent energy relaxation in terms of time-averaged collision frequencies and energy transfer probabilities[23,24] – e.g., isolated binary collision models – may not be accurate in the limit of very short times following (or before) a bimolecular or unimolecular dissociation reaction unless they are modified to account for changes in solvent structural dynamics; and (iii) energy transfer and subsequent chemical reactions that follow on from solution phase bimolecular reactions and unimolecular dissociations in solution are sensitive to the lifetime of solvent caged super-molecular complexes, whose energy transfer properties may be significantly distinct from the bulk on ultrafast timescales.

Recently, Stratt and co-workers[5,10] have argued that the relaxation of rotationally excited CN to equilibrium following ICN photodissociation in an Ar solvent is characterized by two different timescales. The origin of these timescales is related to the efficiency with which the rotationally hot CN is capable of perturbing the solvent structure: at very short times, when the Ar is relatively unperturbed from its equilibrium structure, relaxation is fast, and well-described by LRT. After the hot CN has locally perturbed the solvent structure by effectively carving out a solvent bubble in which it can rotate almost freely, relaxation is significantly slower. This work presents a sort of vibrational analogue to those observations, with HCN relaxation moving between two different regimes depending on the solvent structure in which it is embedded. The goodness of the biexponential fit in Figure 3 suggests that the switching between LRT domains is relatively abrupt.

Sophisticated experimental and theoretical methods are increasingly revealing the details of time resolved chemical dynamics in solution,[19,20,25] in order to better understand how these impact on mode-selective chemistry,[26] biochemistry,[27,28] and the outcomes of chemical reactions.[29,30] In that context, this work represents a step toward revealing fundamental microscopic details of condensed phase thermal reaction dynamics, and delineating appropriate regimes for applying models as widespread as LRT – especially given that the vibrational energies in our system are rather characteristic of typical thermal reaction energies encountered in a wide range of systems spanning synthetic and biochemistry.

Acknowledgment. T. A. A. Oliver, M. N. R. Ashfold, I. P. Clark, G. P. Greetham, A. W. Parker, and M. Towrie for contribution to the experimental work we discuss. Funding was provided by the EPSRC Programme Grant EP/G00224X. We thank the Leverhulme Trust for an Early Career Research Fellowship (S.J.G.) and the Royal Society and the Wolfson Foundation for a Research Merit Award (A.J.O.E).

References

1 Gruebele, M. & Wolynes, P. G. Vibrational energy flow and chemical reactions. *Accounts Chem. Res.* **37**, 261-267 (2004).

2 Stratt, R. M. Chemistry - Nonlinear thinking about molecular energy transfer. *Science* **321**, 1789-1790 (2008).

3 Chandler, D. *Introduction to Modern Statistical Mechanics*. (Oxford University Press, 1987).

4 Turi, L., Minary, P. & Rossky, P. J. Non-linear response and hydrogen bond dynamics for electron solvation in methanol. *Chem. Phys. Lett.* **316**, 465-470 (2000).

5 Moskun, A. C., Jailaubekov, A. E., Bradforth, S. E., Tao, G. H. & Stratt, R. M. Rotational coherence and a sudden breakdown in linear response seen in room-temperature liquids. *Science* **311**, 1907-1911 (2006).

6 Bragg, A. E., Cavanagh, M. C. & Schwartz, B. J. Linear response breakdown in solvation dynamics induced by atomic electron-transfer reactions. *Science* **321**, 1817-1822 (2008).

7 Fonseca, T. & Ladanyi, B. M. Breakdown of Linear Response for Solvation Dynamics in Methanol. *J. Phys. Chem.* **95**, 2116-2119 (1991).

8 Smallwood, C. J., Bosma, W. B., Larsen, R. E. & Schwartz, B. J. The role of electronic symmetry in charge-transfer-to-solvent reactions: Quantum nonadiabatic computer simulation of photoexcited sodium anions. *J. Chem. Phys.* **119**, 11263-11277 (2003).

9 Geissler, P. L. & Chandler, D. Importance sampling and theory of nonequilibrium solvation dynamics in water. *J. Chem. Phys.* **113**, 9759-9765 (2000).

10 Tao, G. H. & Stratt, R. M. The molecular origins of nonlinear response in solute energy relaxation: The example of high-energy rotational relaxation. *J. Chem. Phys.* **125**, 17, doi:114501 10.1063/1.2336780 (2006).

11 Bethardy, G. A., Northrup, F. J. & Macdonald, R. G. The initial vibrational level distribution and relaxation of HCN[X $^1\Sigma^+(v_1,0,v_3)$] in the CN (X $^2\Sigma^+$)+CH_4 □ HCN+CH_3 reaction system. *J. Chem. Phys.* **105**, 4533-4549 (1996).

12 Bethardy, G. A., Northrup, F. J., He, G., Tokue, I. & Macdonald, R. G. Initial vibrational level distribution of HCN[X $^1\Sigma^+(v_1v_3)$] from the CN(X $^2\Sigma^+$)+H_2□HCN+H reaction. *J. Chem. Phys.* **109**, 4224-4236 (1998).

13 Bethardy, G. A., Northrup, F. J. & Macdonald, R. G. The initial vibrational state distribution of HCN X $^1\Sigma^+(v_1,0,v_3)$ from the reaction CN($^2\Sigma^+$)+C_2H_6 □ HCN+C_2H_5. *J. Chem. Phys.* **102**, 7966-7982 (1995).

14 Bethardy, G. A., Wagner, A. F., Schatz, G. C. & terHorst, M. A. A quasiclassical trajectory study of product state distributions from the CN+H_2□HCN+H reaction. *J. Chem. Phys.* **106**, 6001-6015 (1997).

15 Greaves, S. J. *et al.* Vibrationally Quantum-State–Specific Reaction Dynamics of H Atom Abstraction by CN Radical in Solution. *Science* **331**, 1423-1426 (2011).

16 Glowacki, D. R., Orr-Ewing, A. J. & Harvey, J. N. Product Energy Deposition of CN + alkane H Abstraction Reactions in Gas and Solution Phases. *J. Chem. Phys.* (in press).

17 Glowacki, D. R., Paci, E. & Shalashilin, D. V. Boxed molecular dynamics: decorrelation timescales and the kinetic master equation. *J. Chem. Theory Comput.* **7**, 1244-1252 (2011).

18 Glowacki, D. R., Paci, E. & Shalashilin, D. V. Boxed molecular dynamics: a simple and general technique for accelerating rare event kinetics and mapping free energy in large molecular systems. *J Phys Chem B* **113**, 16603-16611 (2009).

19 Owrutsky, J. C., Raftery, D. & Hochstrasser, R. M. Vibrational Relaxation Dynamics in Solutions. *Annu. Rev. Phys. Chem.* **45**, 519-555 (1994).

20 Elles, C. G. & Crim, F. F. Connecting chemical dynamics in gases and liquids. *Annu. Rev. Phys. Chem.* **57**, 273-302 (2006).

21 Dang, L. X. Intermolecular interactions of liquid dichloromethane and equilibrium properties of liquid-vapor and liquid-liquid interfaces: A molecular dynamics study. *J. Chem. Phys.* **110**, 10113-10122 (1999).

22 Laird, B. B. & Thompson, W. H. On the connection between Gaussian statistics and excited-state linear response for time-dependent fluorescence. *J. Chem. Phys.* **126**, 4, doi:211104 10.1063/1.2747237 (2007).

23 Harris, A. L., Brown, J. K. & Harris, C. B. The nature of simple photodissociation reactions in liquids on ultrafast timescales. *Annu. Rev. Phys. Chem.* **39**, 341-366 (1988).

24 Nandi, N., Bhattacharyya, K. & Bagchi, B. Dielectric relaxation and solvation dynamics of water in complex chemical and biological systems. *Chem. Rev.* **100**, 2013-2045 (2000).

25 Voth, G. A. & Hochstrasser, R. M. Transition state dynamics and relaxation processes in solutions: A Frontier of physical chemistry. *J. Phys. Chem.* **100**, 13034-13049 (1996).

26 Crim, F. F. Chemical dynamics of vibrationally excited molecules: Controlling reactions in gases and on surfaces. *Proc. Natl. Acad. Sci. U. S. A.* **105**, 12654-12661 (2008).

27 Noé, F. *et al.* Dynamical fingerprints for probing individual relaxation processes in biomolecular dynamics with simulations and kinetic experiments. *Proc. Natl. Acad. Sci. U. S. A.* **doi: 10.1073/pnas.1004646108** (2011).

[28] Franco, M. I., Turina, L., Mershin, A. & Skoulakisa, E. M. C. Molecular vibration-sensing component in Drosophila melanogaster olfaction. *Proc. Natl. Acad. Sci. U. S. A.* **doi: 10.1073/pnas.1012293108** (2011).

[29] Glowacki, D. R., Liang, C. H., Marsden, S. P., Harvey, J. N. & Pilling, M. J. Alkene Hydroboration: Hot Intermediates That React While They Are Cooling. *J. Am. Chem. Soc.* **132**, 13621-13623 (2010).

[30] Goldman, L. M., Glowacki, D. R. & Carpenter, B. K. Nonstatistical Dynamics in Unlikely Places: [1,5] Hydrogen Migration in Chemically Activated Cyclopentadiene. *J. Am. Chem. Soc.*, Articles ASAP, doi:10.1021/ja1095717.